Contents lists available at ScienceDirect

Petroleum Science

journal homepage: www.keaipublishing.com/en/journals/petroleum-science



Original Paper

Deep original information preservation by applying in-situ film formation technology during coring



Liang-Yu Zhu ^a, Tao Liu ^{b, *}, Zhi-Yu Zhao ^b, Yi-Fan Wu ^b, Dong-Sheng Yang ^c, Xiang-Chao Shi ^{a, **}, Zhi-Qiang Liu ^d, Fei-Fei Lu ^e, Pei Qin ^{f, g}, Xiao-Liang Gao ^e

- ^a State Key Laboratory of Oil and Gas Reservoir Geology and Exploitation, Southwest Petroleum University, Chengdu, 610500, China
- ^b Institute of New Energy and Low-Carbon Technology, Sichuan University, Chengdu, 610065, Sichuan, China
- ^c College of Polymer Science and Engineering, Sichuan University, Chengdu, 610065, China
- ^d Zaoshenzhuang Village, Hancheng Towu, Lubei District, Tangshan, 064002, Hebei, China
- ^e Xi'an Research Institute, China Coal Technology&Engineering Group Corp, Xi'an, 710077, China
- f State Key Laboratory of Coking Coal Exploitation and Comprehensive Utilization, Pingdingshan, 467000, China
- g Institute of Coal Mining and Utilization, Pingdingshan Tianan Coal Mining Co., LTD., Pingdingshan, 467000, China

ARTICLE INFO

Article history: Received 19 July 2021 Accepted 25 January 2022 Available online 1 March 2022

Edited by Xiu-Qiu Peng

Keywords: Deep resource exploitation Original information ISP-IMP-ILP-Coring Solid sealing film In-situ film-forming Film formation during coring

ABSTRACT

Accurately obtaining the original information of an *in-situ* rock via coring is a significant guiding step for exploring and developing deep oil and gas resources. It is difficult for traditional coring technology and equipment to preserve the original information in deep rocks. This study develops a technology for insitu substance-preserved (ISP), moisture-preserved (IMP), and light-preserved (ILP) coring. This technology stores the original information in real time by forming a solid sealing film on the *in-situ* sample during coring, This study designed the ISP-IMP-ILP-Coring process and tool. In addition, an ISP-IMP-ILP-Coring process simulation system was developed. The effects of temperature, pressure, and film thickness on the quality of the in-situ film were investigated by performing in-situ film-forming simulation experiments. A solid sealing film with a thickness of 2-3 mm can be formed; it completely covers the core sample and has uniform thickness. The film maintains good ISP-IMP-ILP properties and can protect the core sample in the *in-situ* environment steadily. This study verifies the feasibility of "film formation during coring" technology and provides strong support for the engineering application of ISP-IMP-ILP-Coring technology.

© 2022 The Authors, Publishing services by Elsevier B.V. on behalf of KeAi Communications Co. Ltd. This is an open access article under the CC BY-NC-ND license (http://creativecommons.org/licenses/by-nc-nd/

4.0/).

1. Introduction

Following the gradual exhaustion of shallow earth resources, the development and exploitation of deep earth resources have become an important strategy for maintaining future resource productivity (Yao et al., 2013; Pang et al., 2015). More than 1,000 deep oil and gas reservoirs (buried depths of 4,500 m to 8,130 m) have been developed all over the world (Sun et al., 2013). Until 2010, the production of deep oil reached 1.21×10^8 and that of deep natural gas reached 1054×10^8 m³ (Li et al., 2021). Recently, there has been great exploration potential for abundant industrial oil and

E-mail addresses: liutao3200023@scu.edu.cn (T. Liu), sxcdream@163.com (X.-C. Shi).

gas reservoirs in Kuqa, Tazhong, Tabei, Yuanba, and Niudong of the Tarim Basin, Sichuan Basin, and Bohai Bay Basin (Tian et al., 2010; Zhao et al., 2013; Sun et al., 2015). The challenges of deep resource development, such as complex formation lithology and pressure systems, in-situ high geostress, temperature, and osmotic pressure environments, have restricted the development of deep resources (Xie et al., 2015; Gao et al. 2018, 2020a, 2020b, 2021a, 2021b, 2022; Xie, 2019). However, the "common core samples" that have been obtained via the current coring technology have lost their actual condition and original information, such as the in-situ pressure, temperature, substance composition, fluid saturation, and microorganism. As a result, assessing the actual condition and original information of in-situ rocks is difficult (Xie et al., 2020). This has necessitated the development of *in-situ* condition-preserved coring (ICP-Coring) technology to determine the actual conditions and original information of deep in-situ rocks, and thereby establish the

^{*} Corresponding author.

^{**} Corresponding author.

Abbreviations

HY-ACE -Hydrate-autoclave coring equipment
ISP -Coring In-situ substance-preserved coring
IMP -Coring In-situ moisture-preserved coring
ILP -Coring In-situ light-preserved coring
ICP -Coring In-situ condition-preserved coring
PCS -Pressure core sampler

theory of deep in-situ rock mechanics and provide theoretical and technical guidance for the development of deep resources. Presently, most traditional coring technologies and equipment focus significantly on maintaining the in-situ temperature and pressure of rocks, and only a little on maintaining the original information in the rock pores. The pollutant contamination from the external environment to the core or the substance exchange with the core is the main reason for the distortion of the original information. This includes the erosion pollution of drilling fluid to the core during the coring process and the constant outward release of components in the pore during the core transfer and testing (Sun et al., 2020). A pressure core sampler (PCS) and hydrate-autoclave coring equipment (HY-ACE) adopt a resin core barrel to ensure close proximity between the core and the resin core barrel during coring to reduce the entry of the drilling fluid into the core barrel. In addition, a piston mechanism is integrated into the core barrel so that the seawater entering the core barrel is discharged through a one-way valve (Hohnberg et al., 2003; Milkov et al., 2004; Bohrmann et al., 2007; Schultheiss et al., 2009; Zhu et al., 2013). These mechanisms can only prevent the drilling fluid from coming into contact with the core, but they do not prevent the drilling fluid from seeping into the rock pores under high-pressure conditions. In the sponge coring process, flexible polyurethane sponge bushing is installed in the core barrel. The sponge bushing is closely attached to the core, preventing the drilling fluid from invading the core pores. However, the original core fluid flows into the sponge bushing from the pores (Shale et al., 2014), and cannot prevent the spread of the original substance during the transfer and testing process; In the sealing coring process, a non-aggressive colloid sealing liquid is present in the core barrel, and the liquid is released while coring to drain the drilling fluid between the core sample and core barrel. The sealing liquid is used to isolate the core sample from the drilling fluid during the coring process. This prevents the direct intrusion of the drilling fluid into the pores of the core sample. However, when the in-situ temperature exceeds 100 °C, the viscosity of the sealing liquid decreases significantly, and the gas and fluid in the core pores cannot be prevented from diffusing into the sealing liquid. Therefore, a correction calculation model for an indirect fluid saturation in the pores of the core sample must be established in the core analysis (Chen et al., 2019; Ma, Li, 2016; Tu, Li, 2017).

To obtain the core samples with fully preserved *in-situ* conditions and information, it is necessary to develop a novel ISP-IMP-ILP-Coring technology (Xie et al. 2020, 2021). In December 2018, our team first proposed the concept and mechanism of deep *in-situ* condition preserved (e.g., heat, pressure, substance, moisture, and light preserved) coring technology (Wan et al., 2019; He et al., 2019; Yu et al., 2020; Li et al., 2020; Gao et al., 2021c). This was done to retain the in-situ environmental conditions of the core sample during the process of coring, transferring, storing, and testing. As the key technology, ISP-IMP-ILP-Coring aims to preserve the deep *in-situ* original information in the pores inside the core sample. ISP-Coring is utilized to preserve the substance in the core sample, especially the volatile gas and liquid components, which is

conducive to accurately identifying the oil and gas reservoir location and the reserve evaluation. IMP-Coring is used to preserve the humidity or the oil and water saturation in the pores inside the core sample, which is crucial to accurately describing the remaining oil distribution in the reservoir during the production process(Zhao, 2021; Iscan, 2021). ILP-Coring is used to maintain the dark environment of the in-situ rock and prevents the external light pollution of the core sample, which is performed to avoid the extinction of microorganisms that may exist, and provide research materials for deep life science (Teske, 2005; Mcmahon, Ivarsson, 2019; Borgonie et al., 2015). Inspired by the phenomenon that an egg is wrapped in an oil sealing film instantly when thrown into the oil, we proposed the concept of "in-situ solid sealing film formation while coring "(Xie et al., 2020; Zhao et al., 2020). As shown in Fig. 1, a polymer film-forming solution is used to protect the *in-situ* core sample while coring. The solution with high viscosity cannot invade the core pores and cause damage to the original fluid. In addition, the solution drains the drilling fluid and prevents pollution of the core sample during the dynamic coring process (Fig. 1a). More importantly, after covering the core surface, the solution triggers the crosslinking reaction and develops into a polymer solid sealing film with a microscopic dense structure. (Fig. 1b). Compared with the sealing liquid, the solid sealing film features an excellent molecule barrier, mechanical performances, and chemical stability; and is light-proof. Therefore, the information in the core pores is completely isolated from the outside environment. The solid sealing film blocks the substance exchange inside and outside the core and preserves the original information inside the core for a long time during the transfer and testing process. Liu et al. also used the same methodology for coring in old wells (Liu et al., 2021).

Based on the conception and principle of the "in-situ solid sealing film formation while coring", this study designed an ISP-IMP-ILP-Coring simulation system with the functions of crosslinking reaction solutions isolation storage and self-triggering premixing. The film formation during the coring process is simulated under the in-situ temperature and pressure environment. In addition, an *in-situ* film with excellent comprehensive performance is obtained on the core sample surface, which verifies the feasibility of the ISP-IMP-ILP-Coring technology. The effects of the in-situ filmforming space, temperature, and pressure on the coverage, thickness uniformity, and comprehensive performance of the in-situ film were investigated. The environmental and technological factors controlling the performance of the in-situ film are analyzed. This provides the basis for the development of film materials and the optimization of the film formation during the coring process. This study will strongly promote the engineering application of deep ISP-IMP-ILP-Coring technology.

2. ISP-IMP-ILP-coring process and tool

To achieve the process of *in-situ* film-formation during coring, the accurate control of the initial time of the liquid-solid phase transformation reaction of the film-forming solution is necessary. When the film-forming solution reaches the bottom of the well from the surface, it must remain in a flowable state for a long time before coring. It is necessary for the film-forming solution to trigger the crosslinking reaction at the beginning of coring. Therefore, we innovatively designed the process that is referred to as the "*in-situ* isolation storage and self-triggered premixing of crosslinking reaction solutions". The components in the film-forming solution producing the crosslinking reaction are divided into two solutions (crosslinking reaction solutions, hereafter referred to as A/B solutions), which are pre-stored in isolation in the core barrel before coring. The A/B solutions can be stably stored separately before they are mixed. At the beginning of coring, the A/B solutions were

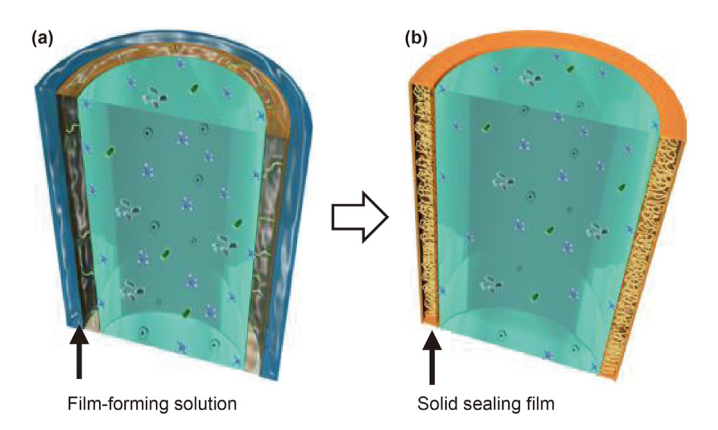


Fig. 1. Schematic of *in-situ* solid sealing film formation **a** before film formation and **b** after film formation.

simultaneously discharged and mixed to form the film-forming solution with the ability of crosslinking curing. Based on this process, we designed an ISP-IMP-ILP-Coring tool. The implementation of the coring process is illustrated in Fig. 2a. The key components of this tool (e.g., a solution reservoir, floating piston, and static mixer) are integrated into the core barrel, which can be run down the bottom hole using a rope and attached to the inner wall of the drill string. There are four groups of reduced-diameter through-holes in the solution reservoir. The upper and lower ends of the throughholes are installed with immobile and floating pistons respectively, forming four groups of isolated solution storage chambers, where the A/B solutions are pre-stored before coring. The bottom of the floating pistons is supported by springs, which separate the solution storage chambers from the confluence channel at the bottom of the solution reservoir, and they can maintain the balance of the fluid pressure inside and outside. During coring (Fig. 2b), the core barrel goes down with the drill bit, and the bearing device at the top prevents the core barrel from rotating. When the core sample enters the core barrel, the solution reservoir is pushed upward and produces relative displacement with the immobile piston. Therefore, the space in the solution storage chamber is reduced, and the pressure of the A/B solutions increases. The floating pistons shift under a pressure difference, and they connect the four solution chambers with the confluence channel. The A/B solutions are simultaneously extruded into the confluence channel, and the film-forming solution is formed after premixing with the static mixer in the confluence channel. As a result, the crosslinking curing reaction is initiated by the dynamic coring process, which successfully controls the initial time of the cross-linking and curing reaction of the film-forming solution. The film-forming solution covers the top and side surface of the core sample while drilling, forming a protective area that allows for the isolation of the drilling fluid. A resilient packer with a petal structure is installed at the bottom of the core barrel, which spreads when the core sample enters the core barrel, and automatically springs back and closes as the core sample completely enters the core barrel. The film-forming solution rapidly crosslinks to form a solid sealing film over the surface of the core sample; therefore, the bottom of the core barrel is sealed (Fig. 2c). As such, the core sample is completely sealed in the film, thereby ensuring the core sample can be protected continuously and in the long-term.

3. Deep ISP-IMP-ILP-coring simulation system

We built a simulation system based on the ISP-IMP-ILP-Coring process. The structure is divided into a film-forming simulation chamber and an external control module. They can be coordinated to verify the film formation during the coring process in an *in-situ* high-temperature and high-pressure environment.

The film-forming simulation chamber simulates film-formation during the coring process in a narrow space through its mechanical structure. The main internal components are shown in Fig. 3a and b, and include the piston-rod combination, core barrel, solution reservoir, and its internal floating pistons and static mixers. The solution reservoir has four cylindrical storage chambers with a diameter of 20 mm and a length of 110 mm, and the liquid storage capacity can reach 138 ml. The core with a length of 100 mm and diameter of 50 mm is located in the sleeve below the core barrel with a piston-rod combination at the bottom. The top and bottom of the core are fitted with a bonnet with several flow channels with

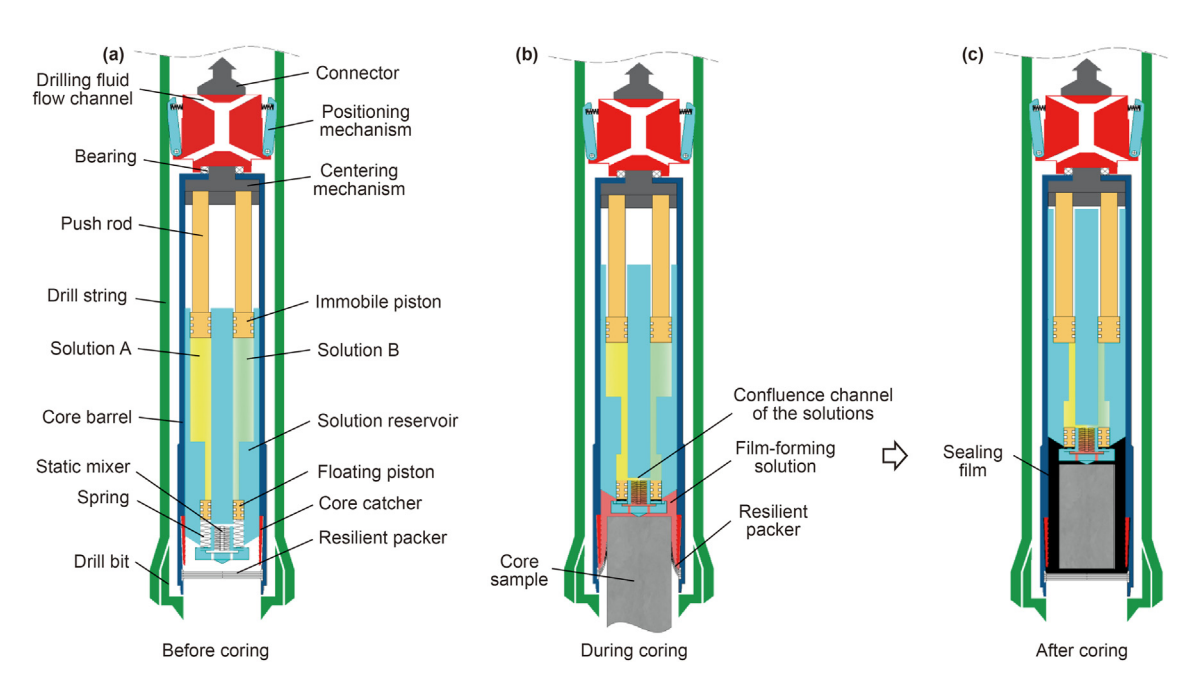


Fig. 2. Schematic of ISP-IMP-ILP-Coring ${\bf a}$ before coring, ${\bf b}$ during coring, and ${\bf c}$ after coring.

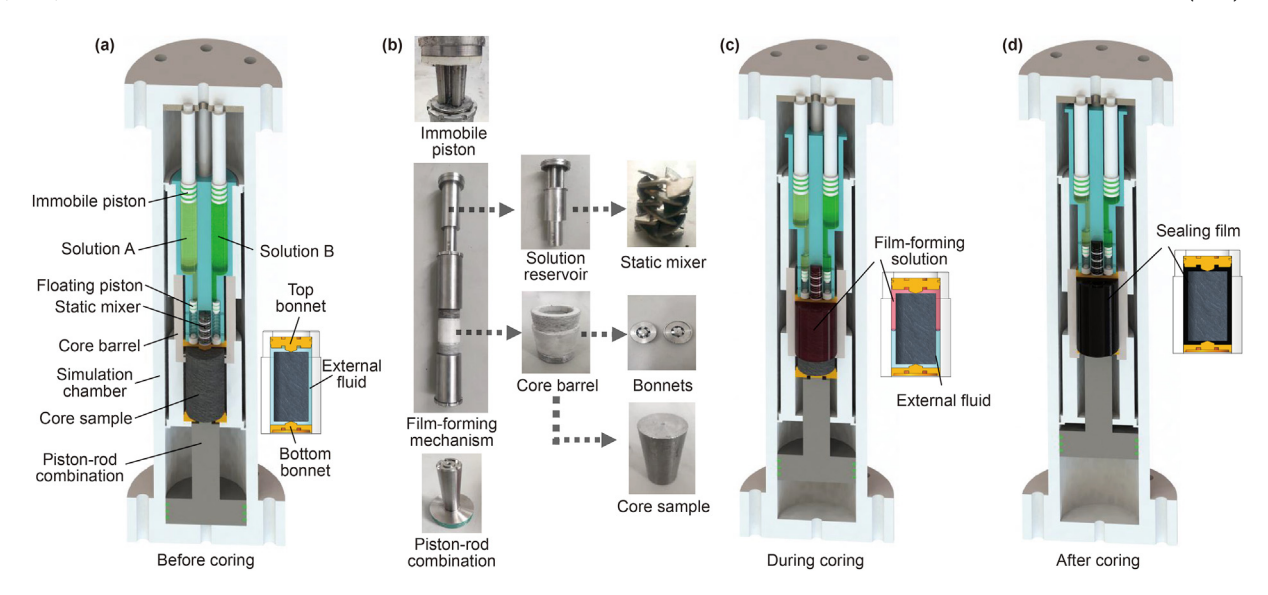


Fig. 3. Schematic of the simulated ISP-IMP-ILP-Coring process a before simulation coring, b internal components, c during simulation coring, d and after simulation coring.

a diameter of 3 mm. The bonnet is in point contact with the core sample and has the same size as the inner diameter of the core barrel so that the core sample is centered. The thickness of the film generated on the core surface can be controlled by adjusting the inner diameter of the core barrel. When the simulated coring begins (Fig. 3c), the piston-rod combinations push the bonnets and core upward into the core barrel for 110 mm. The solution reservoir was driven further to move upward, and the A/B solutions were extruded into the cylindrical confluence channel with a diameter of 16 mm and a length of 50 mm by the relative motion of the immobile piston. After being premixed with a static mixer, a filmforming solution was formed. The film-forming solution passes through the flow channel of the bonnets and covers the core sample while coring. This forms a protected area around the core that isolates the external fluid. The film-forming solution rapidly crosslinks and finally forms a solid sealing film on the surface of the core sample (Fig. 3d).

The static mixer plays a significant role in the *in-situ* premixing process, where the A/B solutions are uniformly premixed and dispersed to form a film-forming solution in the confluence channel. If the A/B solutions cannot be uniformly premixed and dispersed, the components in the A/B solutions cannot come into full contact and react. Accordingly, there will be a large amount of free volume and residual small molecules or oligomers in the in-situ film owing to the incomplete polymerization. This results in a decrease in the comprehensive performance of the film and the ISP-IMP-ILP ability. Because of the narrow space of the confluence channel (50 \times Φ 16 mm), the premixing travel and time of the A/B solutions are limited; hence, obtaining a uniformly dispersed filmforming solution is difficult. Therefore, we designed a special static mixer with an outer diameter of 16 mm, which comprises impeller mixer units and necking mixer units, as shown in Fig. 4. The impeller mixer units were superimposed in the positive and negative deflection directions. Because the two adjacent impellers deflect in opposite directions, the flow direction of the fluid between them constantly changes. When the A/B solution passes through the impeller blade, it goes through the cut, refined, and dispersed process to form multiple bundles of fluid that flow downward along the deflection direction of the impeller. A 3 mm shrinkage channel in the middle of the necking mixer unit forces the A/B solutions to converge from the periphery to the center for contact and integration. This causes impact, shear, and

recombination between the flows. At the same time, the flow direction, velocity, and pressure change dramatically when they pass through the shrinkage channel, which increases the probability of interflow between the A/B solutions. The impeller and necking mixer units were superimposed and combined at a ratio of 4:1 to form the special static mixer used. This can effectively premix and disperse the A/B solutions in the *in-situ* narrow space.

The external control module of the simulation system can restore the deep *in-situ* coring condition of high levels of temperature and pressure; the image and schematic are shown in Fig. 5. The simulation temperature ranges from 30 to 150 °C and the pressure from 0 to 10 MPa (manometer pressure); the internal medium fluid can be water, oil, or drilling fluid. The control center can control the experimental temperature fluctuation within 1 °C and the pressure fluctuation within 0.1 MPa. Before the simulation started, the film-forming mechanism was first loaded into the simulation chamber. Subsequently, the medium liquid was injected into the chamber through the piston pump by liquid inlet 1 to simulate the fluid environment during coring. The simulation chamber was then heated to a predetermined value using the heating apparatus, and the medium liquid was injected from liquid

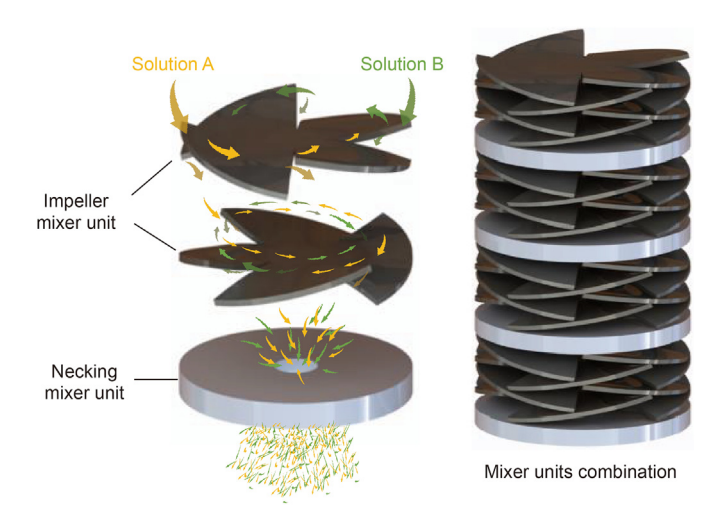


Fig. 4. Schematic of the special static mixer.

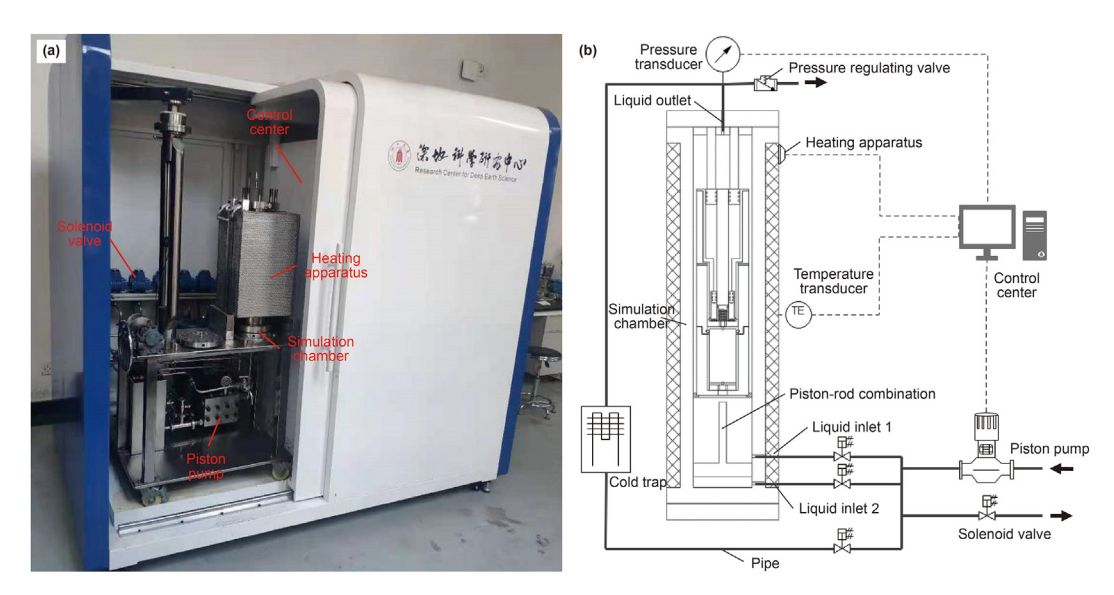


Fig. 5. a External control module. b Schematic of the external control module.

inlet 2 to push the piston-rod combination upward. Afterwards, the core was pushed into the core barrel. To simulate actual coring speed, the pushing speed can be controlled within 0.2–3 mm/s by changing the liquid injection displacement of the piston pump. In this process, the piston-rod combinations pressurize the uppermedium liquid, and the opening pressure of the pressure-regulating valve at the liquid outlet can be adjusted arbitrarily within the range of 0–10 MPa. When the hydraulic pressure approaches the opening pressure, the medium liquid is discharged automatically to maintain the hydraulic pressure in the chamber, which is the experimental pressure. After the simulation coring, the simulation chamber was rapidly cooled by circulating the medium liquid in the cold trap pipeline.

4. Experiments

4.1. Materials

A polyurethane modified epoxy resin was used as the raw material of solution A. A mercaptan curing agent, ester cyclic curing agent, and anhydride curing agent were used as the raw materials of solution B, respectively. A diluent was used to regulate the viscosity of the curing agent. The aforementioned chemical reagents were purchased from the Chuzhou Huisheng Electronic Materials Co., Ltd and modified preliminarily. The graphene was purchased from the Deyang Diene Carbon Technology Co., Ltd. and was used for filling in the A/B solutions to improve the barrier and light-proof performance of the film.

4.2. Methods

4.2.1. Preparation of the A/B solutions

In this experiment, 20 g of polyurethane modified epoxy resin and graphene (1 wt%) were added to a polypropylene (PP) plastic beaker and mixed in a vacuum degasser mixing machine for 9 min as solution A. A curing agent of the same quality and a diluent of 5 wt% were added to the beaker and mixed in a vacuum degasser mixing machine for 9 min at room temperature as solution B.

4.2.2. Preparation of the standard film

In this part of the experiment, 10 g of solutions A and B were added to a beaker and mixed in a vacuum degasser mixing machine

for 3 min as the film-forming solution. This was cured at the corresponding temperature for approximately 30 min. The uncured film-forming solution was slowly poured onto a flat polytetra-fluoroethylene plate and coated with a film coating device into a 1 mm film. The cured film was prepared into a Φ 100 mm round sample, used to detect the water vapor and oxygen permeability of the standard film. The film-forming solution was slowly poured into the tensile specimen molds to form the GB/T 1040-92 I standard tensile test specimens, which were used to test the mechanical properties of the standard film. Approximately 1 g of the cured film was placed in saturated salt water to detect the water absorption by the standard film.

4.2.3. Preparation of the in-situ film

During this experiment, 60 g of solutions A and B were loaded into the solution storage chambers in the solution reservoir of the simulation chamber. The core barrel with annular clearances of 0.5, 1, 2, and 3 mm that formed with the core sample was selected for the simulated film-forming experiment. First, the medium liquid was circulated to fill the simulation chamber, and the experimental temperatures (30 °C, 60°C, 90°C) and pressures (0 MPa, 4 MPa, 8 MPa) were set in the control center of the simulation system. After the temperature and pressure were stabilized, the piston-rod combinations pushed the core sample into the core barrel. The A/B solution was discharged from the solution reservoir in a simulated *in-situ* environment. After *in-situ* premixing with the static mixer, the medium liquid around the core sample was displaced by the film-forming solution from top to bottom to form an in-situ film layer. After waiting for 30 min, the simulation chamber was rapidly cooled through a cold trap. Approximately 1 g of the cured film was placed in saturated salt water to detect water absorption by the insitu film.

Solutions A and B were placed inside A/B solution storage chambers. By applying pressure, they were premixed with a static mixer to form a film-forming solution. The film-forming solution was slowly poured onto a flat polytetrafluoroethylene plate and used to form a 1 mm film coating with a film coating device at the *in-situ* temperature. The cured film was prepared into a Φ 100 mm round sample, which was used to detect the water vapor permeability and oxygen permeability of the *in-situ* film. The film-forming solution was slowly poured into the tensile specimen molds to form the GB/T 1040-92 I standard tensile test specimens, which were

used to test the mechanical properties of the *in-situ* film.

4.3. Analysis

To ensure that the ISP-IMP-ILP film-forming process can adapt to the deep *in-situ* environment and realize the engineering application, we assumed that the *in-situ* film must meet multiple indexes. (1) The film that forms on the core sample is thin, complete, and uniform, and the film thickness deviation is less than 10%. (2) By adapting to the *in-situ* high-temperature and high-pressure conditions, *an in-situ* film can be formed under an environment within a temperature range of 0–90°C and pressure range of 0–8 MPa. (3) The comprehensive performance of the *in-situ* film is stable, which can continuously seal and protect the *in-situ* core sample.

Therefore, through the simulation system, we carried out a single-factor variable simulation film formation experiment, as shown in Table 1. This continuously optimizes the ISP-IMP-ILP film formation during the coring process, which is expected to cover the core sample with a complete and uniform solid sealing film under the in-situ temperature and pressure environments. First, under normal temperature and pressure conditions (30 °C, 0 MPa), we controlled the film-forming space by changing the inner diameter of the core barrel to form films with varying thicknesses (0.5, 1, 2, and 3 mm) on the core sample. The film coverage and thickness uniformity were investigated for different film-forming spaces. By optimizing the size of the film-forming space, a thin and uniform film layer formed on the core surface. Furthermore, simulation experiments were carried out at different *in-situ* temperature levels (30, 60, and 90°C) and pressure levels (0, 4, and 8 MPa). These were performed to explore the effect of the in-situ temperature and pressure on the film coverage and thickness uniformity. All the studies verified the feasibility of implementing the ISP-IMP-ILP film-forming process in engineering.

In addition, the *in-situ* film that was generated by *in-situ* premixing under simulated high-temperature and high-pressure environments (90°C, 8 MPa) was compared with the standard film. The effect of the processes of "*in-situ* isolation storage and self-triggered premixing of crosslinking reaction solutions" on the *in-situ* crosslinking curing degree of the film-forming solution and the comprehensive properties of the *in-situ* film were investigated. This provided the basis and a reference for the development of the sealing film material and the optimization of the ISP-IMP-ILP film-forming process.

An oxygen permeability analyzer (Y310, GBPI Co., Ltd.) was used

to test the oxygen permeability of the film to characterize the ISP performance of the *in-situ* film. The test sample was required to be a circular sheet with a diameter of 100 mm. The contact surface between the sample and the test fixture was smeared with vacuum silicone grease to prevent gas leakage. The oxygen and nitrogen pressures were adjusted to 0.1 MPa, and the test temperature was controlled at 23 °C. The test was concluded when the straight test curve leveled off, and at least three data points fluctuated within 5%.

A water vapor permeability analyzer (W403, GBPI Co., Ltd.) was used to test the water vapor permeability of the film to characterize the IMP performance of the in-situ film. The test temperature was controlled at 38 °C during the test. The test ended when the straight test curve leveled off, and at least three data points fluctuated within 5%.

The light flux of the film was measured using a light transmittance and haze tester (SGW-810 model, GBPI Co., Ltd.) to characterize the ILP performance of the film. The light transmittance was measured at 30°C and humidity below 60%. After preheating the instrument, the prepared square sample (100 mm \times 100 mm) was placed on the sample holder for the transmittance measurement.

Tensile tests were carried out on an AGS-J testing machine manufactured by the Shimazu Company in Japan to test the stability of the film against mechanical damage. The experimental environment of the samples was prepared under the provisions of GN2918, and the loading speed of the samples in the tensile test process was set at 4 mm/min.

Approximately 1 g of the film was placed in saturated salt water. The mass change rate of the film was measured using an electronic balance manufactured by the Hangzhou Wante Weighing Equipment Co., Ltd., to characterize the water absorption of the film. The measurement accuracy was 0.01 g, and the measurement intervals were 0, 6, 24, 48, and 96 h. The film was weighed three times, and the average value for each measurement was determined.

A Nova Nano SEM450 scanning electron microscope (FEI Company, USA) was used to observe the surface and section morphology of the film under a 5 kV acceleration voltage. First, the prepared film was slightly cut and immersed in liquid nitrogen for 5 min. A tweezer was used to clamp the brittle break of the film and mark the section. Before observation, all the samples were sprayed with gold; they were attached to the sample table of the scanning electron microscope through a conductive adhesive. Afterwards, they were placed in the sample chamber to scan the sample surface and section.

Table 1 Film-forming experiment scheme.

Number	Thickness, mm	Curing agent	Temperature, °C	Pressure, MPa
1	0.5	Mercaptans(100%)	30	0
2	1	Mercaptans(100%)	30	0
3	2	Mercaptans(100%)	30	0
4	3	Mercaptans(100%)	30	0
5	2	Mercaptans(100%)	60	0
6	2	Mercaptans(100%)	90	0
7	2	Mercaptans(80%)	60	0
		Anhydrides(20%)		
8	2	Mercaptans(40%)	90	0
		Anhydrides(60%)		
9	2	Mercaptans(40%)	90	4
		Anhydrides(60%)		
10	2	Mercaptans(40%)	90	8
		Anhydrides(60%)		

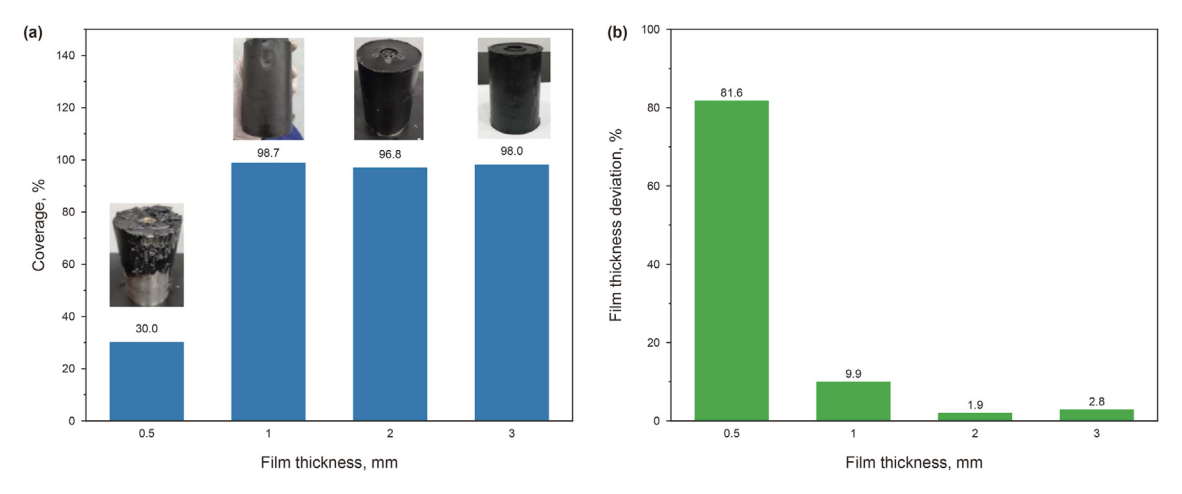


Fig. 6. a Film coverage in different film-forming spaces. b Film thickness deviation in different film-forming spaces.



Fig. 7. a Demolding process of the film-forming core sample. b Film-forming core sample at 30°C, 60°C and 90°C. c In-situ impeller mixer units.

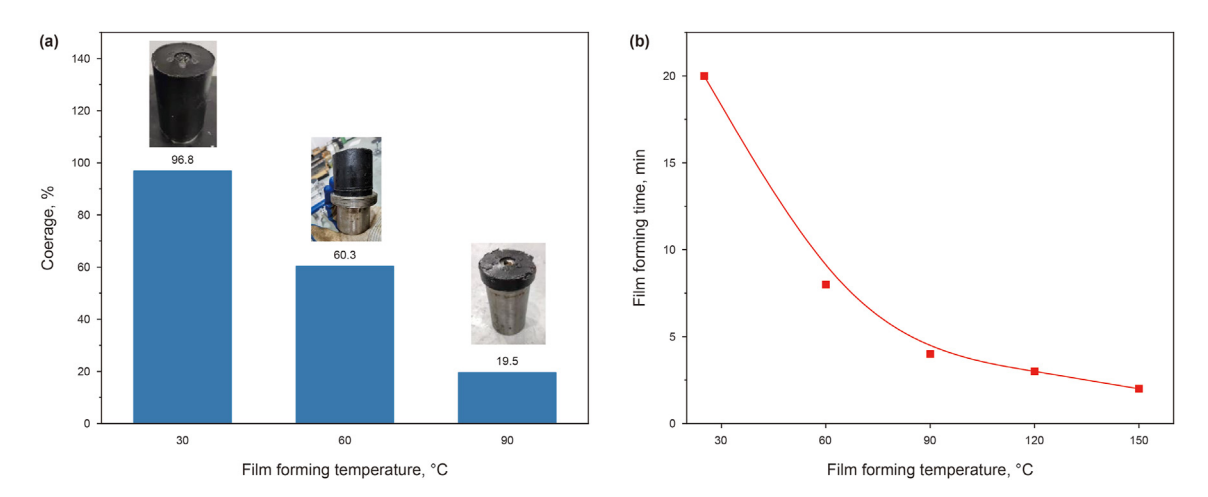


Fig. 8. a Film coverage for the different *in-situ* temperatures with the mercaptan curing agent. **b** Curing time of the film-forming solution with the mercaptan curing agent that varies with temperature.

5. Results and discussion

5.1. Effect of the in-situ film-forming space on the film-forming process

The effect of the different film-forming spaces on the *in-situ* film was investigated under the experimental conditions of 30 °C and 0 MPa. The coverage (film covered area/total core sample surface area) was used to evaluate the *in-situ* film completeness, and film thickness deviation rate (film thickness deviation value/annulus

space width) was used to evaluate the *in-situ* film uniformity. As depicted in Fig. 6a, in the annulus space of 1/2/3 mm, the filmforming fluid can completely cover the top, side, and bottom surface of the core. In addition, the coverage was high: 98.7%, 96.8%, and 98.0%, respectively (as the bonnets exert a driving force and a centralizing force on the top and bottom of the core, the contact site cannot cover the film layer, and the film coverage cannot reach 100%; these will be improved in subsequent studies). However, when the film is formed in the annulus space (0.5 mm), the displacement interface drainage velocity in the annulus is uneven

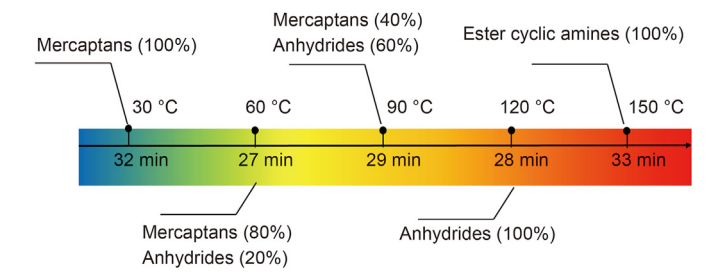


Fig. 9. Combination of the curing agents in the full temperature stage.

because of the narrow annulus flow channel and the eccentricity of the core sample. Following the increase in the core sample eccentricity, the displacement efficiency of the section in the wide gap did not change significantly, whereas the efficiency of the section at the narrow gap decreased sharply, and the channeling phenomenon occurred. The external fluid easily stays in the core barrel and eventually remains on the core surface. A large area of the core samples was not covered by the sealing film and the coverage was only 30%. The thickness uniformity of the in-situ film was further investigated, and the results are displayed in Fig. 6b. In the 2-3 mm annular space, the film uniformity was higher, and the film thickness deviation rates were 1.9% and 2.8%, respectively. However, in the 1 mm and 0.5 mm annular space, the deviation rate of the insitu film increased to 9.9% and 81.6%. This reflects the effect of the core sample eccentricity on the film thickness deviation that intensified as the film-formation space decreased.

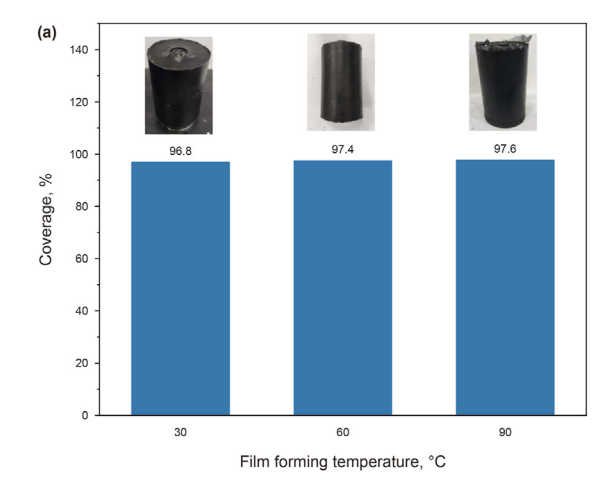
5.2. Effect of the in-situ temperature on the film-forming process

The *in-situ* temperature affects the crosslinking curing rate of the film-forming solution and directly affects the film coverage on the core surface. We used a mercaptan curing agent to carry out the film-forming experiment while coring at 30, 60, and 90 °C. The actual film-forming core samples are shown in Fig. 7a and b. The results demonstrate that the core sample surface can only be covered with a dense and complete solid sealing film at the low-temperature stage (approximately 30 °C), and the coverage is 96.8% (Fig. 8a). Following the increase in the *in-situ* temperature, the coverage decreased from 96.8% to 19.5% because the polymerization activity increased significantly as the *in-situ* temperature increased, and the

crosslinking reaction in the film-forming solution accelerated sharply. As shown in Fig. 8b, when the temperature increased from $20\,^{\circ}\text{C}$ to $150\,^{\circ}\text{C}$, the curing time of the film-forming solution with the mercaptan curing agent plummeted from 20 min to 2 min. Before the core sample completely entered the core barrel, the viscosity of the film-forming solution increased sharply at high temperatures, gelatinized, and solidified, blocking the narrow space of the confluence channel. The A/B solutions could not discharge from the solution reservoir; thereby resulting in a sudden pressure that flattened the static mixer (Fig. 7c). As a result, the resistance of the core sample into the core barrel increased, and it was difficult to enter the core barrel and be film-coated completely.

Therefore, the curing time of the film-forming solution should not be too short at any *in-situ* temperature. However, if the filmforming solution solidifies too slowly and remains in a liquid state for a long time after the completion of coring, preventing the outward loss of small molecules in the core sample becomes difficult, which can affect the sealing. Therefore, we regulated the crosslinking curing time of the film-forming solution in 30 min (coring process time), such that the liquid-solid phase transformation process of the film material could be coupled and matched with the dynamic coring process. To address the variation in the curing rate of the film-forming solution at unique temperatures, a study on the adaptability of the film-forming solution over the entire temperature range was carried out. By performing experiments, three types of curing agents (mercaptans, anhydrides, and ester cyclic amines) were optimized. Finally, a controllable film-forming time (approximately 30 min) over the entire temperature range (30–150 °C) was achieved by combining the curing agents (Fig. 9).

Additional film-forming experiments were carried out at 30, 60, and 90 °C using a film-forming solution with a suitable curing agent. The results showed that the composite film-forming solution formed a complete film layer with a thickness of 2 mm on the surface of the core sample, and the film coverage was 96.8, 97.4, and 97.6%, respectively (Fig. 10a). The thickness deviation rate ranged between 1.9 and 6.5% (Fig. 10b), and the uniformity was remarkable. Through the optimization of the curing agent combination, the applicable temperature range of the film formation during the coring process was effectively extended, thereby providing a basis for the *in-situ* film-forming experiment that was coupled with the high temperature and pressure.



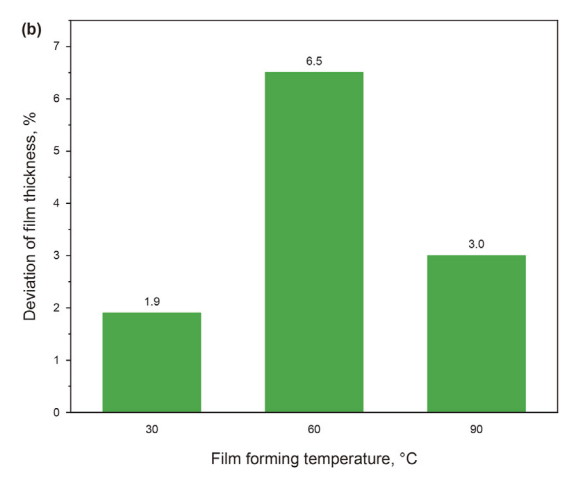


Fig. 10. a Film coverage for the different *in-situ* temperatures with the compound curing agent. **b** Film deviation for the different *in-situ* temperatures with the compound curing agent.

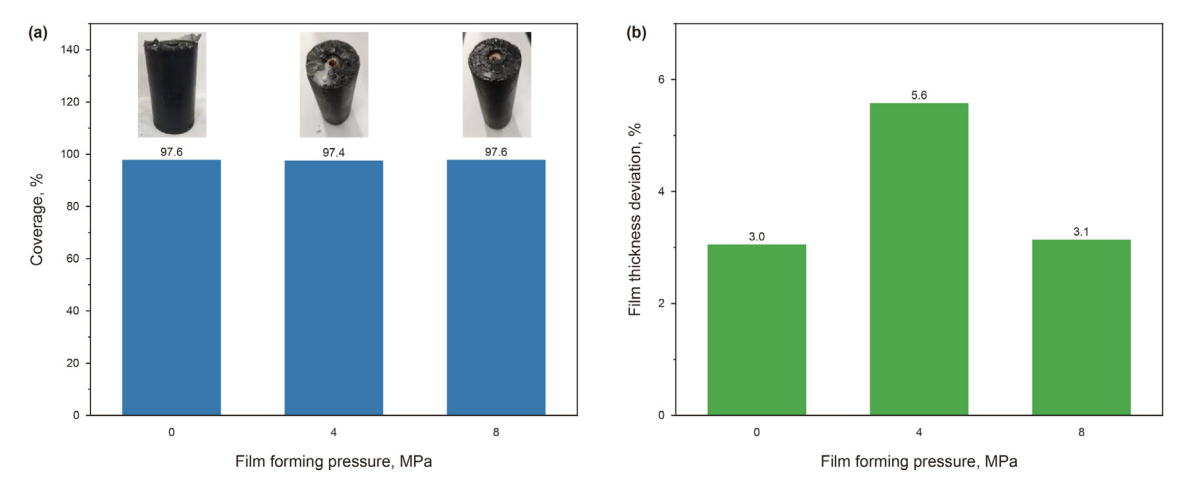


Fig. 11. a Film coverage for the different in-situ pressures. b Film deviation for the different in-situ pressures.

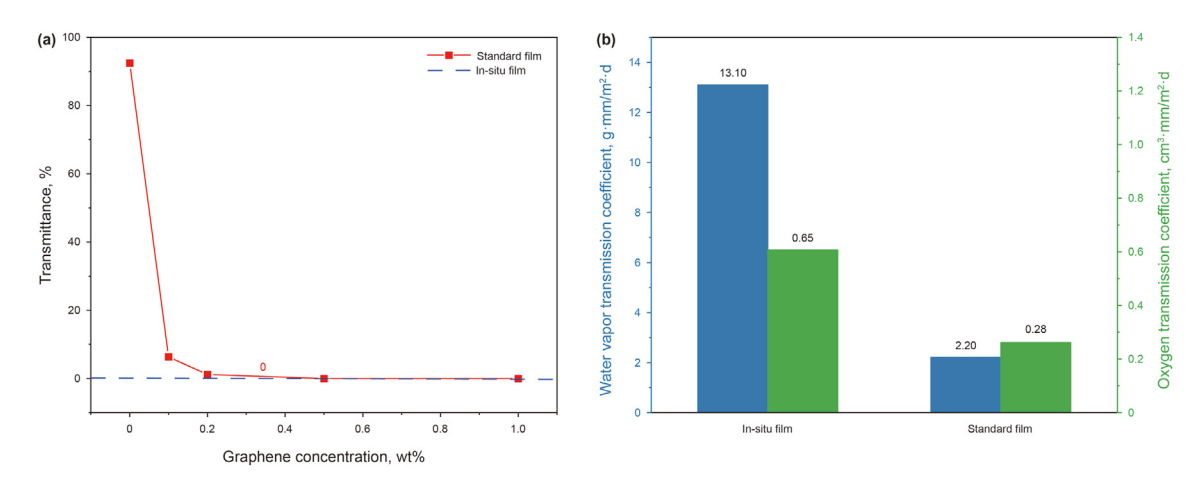


Fig. 12. ISP-IMP-ILP performance of the *in-situ* film and the standard film. a Light flux of the *in-situ* film and standard film. b Barrier performance of the *in-situ* film and standard film.

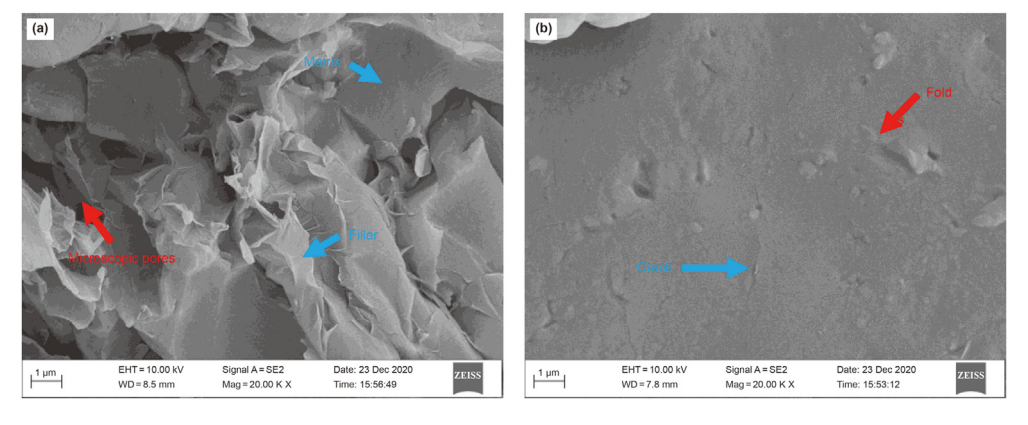


Fig. 13. a SEM image of the cross-section of the in-situ film. b SEM image of the surface of the in-situ film.

5.3. Effect of the in-situ pressure on the film-forming process

The effects of the different *in-situ* pressures (0, 4, and 8 MPa) on the film-forming process were investigated at 90 $^{\circ}$ C and a film-forming space of 2 mm. The results showed that a dense solid layer could be formed on the surface of the core under different pressures. As shown in Fig. 11a, the film coverage at 0, 4, and 8 MPa was high, reaching 97.6, 97.4, and 97.6%, respectively. As shown in

Fig. 11b, the film thickness deviations were 3.0, 5.6, and 3.1%, respectively. The *in-situ* film exhibited remarkable uniformity, indicating no severe eccentricity of the core sample under the simulated pressure. The simulation results showed that the *in-situ* film-forming processes can adapt to conditions under different pressures, and the film was coated in a stable manner on the core surface.

In conclusion, the completeness and uniformity of the in-situ

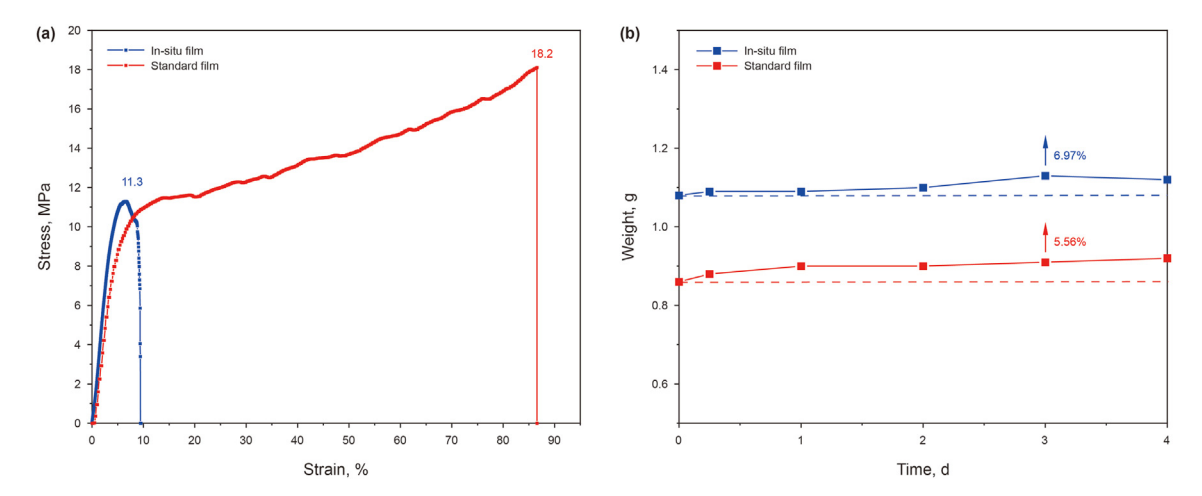


Fig. 14. a Tensile strength of the in-situ film and standard film. b Water absorption rate of the in-situ film and standard film.

film is primarily affected by the eccentricity of the core sample. As the annular film formation space decreases, the degree of the core sample eccentricity tends to increase, thereby adversely affecting the *in-situ* film. In this study, we conclude that 2–3 mm is the appropriate annular space. In addition, temperature determines the crosslinking curing time of the film-forming solution and indirectly affects the *in-situ* film. Through the investigation and control of the crosslinking curing time (approximately 30 min), *in-situ* film can form well at a wide temperature range (30–150 °C). When the crosslinking curing time of the film-forming solution is confirmed, the *in-situ* film-forming processes are minimally affected by temperature and pressure.

5.4. Effect of the in-situ premixing and film formation process on the comprehensive performance of the in-situ film

The in-situ film with 2 mm thickness was fabricated at 90 °C and 8 MPa to comprehensively characterize its performance, and was compared with the standard film. The light transmittance, oxygen permeability coefficient, and water vapor permeability coefficient of the *in-situ* film were maintained at 0 (Figs. 12a), 0.65 cm³/ (m² · d) and 13.1 g/($m^2 \cdot d$) (Fig. 12b), which maintained an excellent ISP-IMP-ILP performance. However, the oxygen and water vapor permeability coefficient of the in-situ film were 2.32 and 5.95 times those of the standard film, indicating that the ISP-IMP performance was reduced. To explain the obvious reduction of the *in-situ* film in the barrier property, a SEM image of the film cross-section was obtained (Fig. 13a). In the film-forming solution, the graphene nanosheet filler was added to the polymer matrix. The filler, acting like a "barrier wall" lengthened the molecular diffusion path and decreased the permeability. However, there were microscopic pores between the filler and the matrix in the in-situ film. This was because the filler was not uniformly dispersed and insufficiently integrated with the matrix in the in-situ premixing process. In addition, because the in-situ premixing process cannot be carried out in a vacuum environment, microbubbles in the film-forming solution cannot be completely removed, such that there were stomatal defects in the in-situ film. As a result, the transfer gas molecule path in the in-situ film was shortened, and the obstruction was reduced; thereby attenuating the in-situ film barrier performance.

The *in-situ* film is considered to be in an adverse environment after forming on the core surface. To ensure that the *in-situ* film can protect the core over long periods, the film material should have good mechanical properties to prevent damage to the *in-situ* film

during the migration and demolding process. In addition, the insitu film must be able to resist water erosion. Therefore, the tensile strength and water absorption rate of in-situ film were measured to explore the stability of the continuous core sample protection by the film in-situ state. As shown in Fig. 14a, the in-situ film tensile strength was maintained at 11.3 MPa, which can resist the mechanical disturbance underground and prevent sealing failure caused by film damage. However, the tensile strength was 37.9% lower than that of the standard film (18.2 MPa). This is because the contact time, mixing travel, and mass transfer area of the A/B solutions in the confluence channel were far lower than those in the vacuum degasser mixing machine; therefore, a thorough dispersion of the A/B solutions in the *in-situ* static mixer was insufficient. The degree of in-situ crosslinking of the in-situ film was reduced locally. The polymer crosslinking network structure was not fully constructed, and there were a few microscopic pores. In addition, micro-cracks and uneven folds appeared on the surface of the insitu film during the film formation and demolding process (Fig. 13b). These occurrences caused a decrease in the mechanical strength of the in-situ film. The water absorption of the in-situ film (6.97%) was 1.25 times higher than that of the standard film (5.56%) (Fig. 14b); however, it was still stable in the in-situ fluid environment. This is because there were a few microscopic pores between the filler and the matrix of the in-situ film (Fig. 13a); thereby, resulting in a decrease in the film density and an increase in the free volume that could allow for water entry.

The *in-situ* film that was formed by "*in-situ* film formation during coring" technology in the simulated deep high temperature and pressure environment maintained excellent ISP-IMP-ILP performance, and the core sample was sealed and preserved stably. The *in-situ* premixing degree of the film-forming solution significantly influences the final comprehensive properties of the *in-situ* film. To improve the ISP-IMP-ILP efficiency for the *in-situ* core samples, it is necessary to optimize the performance of the film material, and to continuously improve the static mixer structure to enhance the *in-situ* premixing degree of the film-forming solution and the display efficiency of the actual performance of the film material in the *in-situ* environment.

6. Conclusions and future prospects

This study designed a deep ISP-IMP-ILP process and tool and proposed a process and mechanism of *in-situ* isolation storage and self-triggered premixing of crosslinking reaction solutions. A deep ISP-IMP-ILP-Coring simulation system was developed to simulate

film formation process *in-situ* high-temperature and high-pressure environments. The effects of the in-situ film-forming space, temperature, and pressure during the film formation process were investigated. Finally, uniform and complete in-situ films under an in-situ temperature (30/60/90 °C) and pressure (0/4/8 MPa) with a thickness of 2/3 mm were formed on the core sample. The effect of "in-situ premixing and film formation during the coring" process on the comprehensive performance of the *in-situ* films was examined in a simulated deep environment. The performance of the in-situ film that was formed at 90 °C and 8 MPa was compared with the standard film. The results showed that the light flux of the in-situ film remained at 0. The oxygen permeability coefficient and water vapor permeability coefficient were 2.32 and 5.95 times the standard film, respectively. In general, the ISP-IMP-ILP performance of the in-situ film was maintained at a suitable level. The mechanical strength of the film was 0.84 times that of the standard film, and the water absorption was 1.25 times that of the standard film. There was only a slight difference in performance, indicating that the insitu film had high performance stability.

This study verified the feasibility of the ISP-IMP-ILP film formation while applying coring technology in engineering applications. In future, our team will continue to explore the mixing mechanism of the static mixer, improve the degree of *in-situ* premixing and dispersion of the film-forming solution, and optimize the ISP-IMP-ILP process. We will develop the ISP-IMP-ILP-Coring simulation system with an optimized process and the ability to simulate the *in-situ* environment at 140 MPa and 150 °C, to ensure that a layer of complete and uniform film can be formed on the core sample surface while coring in deep formations. Further research will promote the development and application of deep ISP-IMP-ILP technology in engineering.

Declaration of competing interest

The authors declare that they have no conflicts of interest.

Acknowledgments

The authors gratefully acknowledge the National Natural Science Foundation of China (grant numbers 51827901, 52004166). This project was also funded by the Program for Shenzhen Basic Research Program (General Program) (No. JCYJ2019080815 3416970) and Guangdong Introducing Innovative and Enterpreneurial Teams (No. 2019ZT08G315).

References

- Bohrmann, G., Kuhs, W.F., Klapp, S.A., et al., 2017. Appearance and preservation of natural gas hydrate from Hydrate Ridge sampled during ODP Leg 204 drilling. Mar. Geol. 244 (1–4), 1–14. https://doi.org/10.1155/2020/8894286.
- Borgonie, G., Linage-Alvarez, B., Ojo, A.O., et al., 2015. Eukaryotic opportunists dominate the deep-subsurface biosphere in South Africa. Nat. Commun. 6, 8952. https://doi.org/10.1038/ncomms9952.
- Chen, D.P., Xue, L., Wang, N., et al., 2019. Semi-analytical correction of three-phase fluid saturation for pressure coring. Special Oil Gas Reservoirs 26 (2), 82–85 (in Chinese).
- Gao, M.Z., Chen, L., Fan, D., et al., 2021c. Principle and technology of coring with insitu pressure and gas maintaining in deep coal mine. J. China Coal Soc. 46 (3), 885–897 (in Chinese).
- Gao, M.Z., Hao H, C., Xue S, N., 2022. Discing behavior and mechanism of cores extracted from Songke-2 well at depths below 4,500 m. Int. J. Rock Mech. Min. Sci. 149.
- Gao, M.Z., Liu J, J., Lin W, M., et al., 2020a. Study on in-situ stress evolution law of ultra-thick coal seam in advance mining. Coal Sci. Technol. 48 (2), 28–35 (in Chinese).
- Gao, M.Z., Xie, J., Gao, Y.N., 2021a. Mechanical behavior of coal under different

- mining rates: a case study from laboratory experiments to field testing. Int. J. Min. Sci. Technol. 31 (2021), 825–841 (in Chinese).
- Gao, M.Z., Xie, J., Guo, J., et al., 2021b. Fractal evolution and connectivity characteristics of mining-induced crack networks in coal masses at different depths. Geomech.Geophys.Geo-Energy.Geo-Resour. 7 (1). https://doi.org/10.1007/s40948-020-00207-4.
- Gao, M.Z., Zhang, J.G., Li, S.W., et al., 2020b. Calculating changes in fractal dimension of surface cracks to quantify how the dynamic loading rate affects rock failure in deep mining. J. Cent. S. Univ. 27 (10), 3013–3024. https://doi.org/10.1007/s11771-020-4525-5.
- Gao, M.Z., Zhang, Z.L., Xiangang, Y., et al., 2018. The location optimum and permeability-enhancing effect of a low-level shield rock roadway. Rock Mech. Rock Eng. 51 (9), 2935–2948. https://doi.org/10.1007/s00603-018-1461-x.
- He, Z.Q., Chen, L., Lu, T., et al., 2019. The optimization of pressure controller for deep earth drilling. Therm. Sci. 23, 123. https://doi.org/10.2298/TSCI180612123H.
- Hohnberg, H.J., Amann, H., Abegg, F., et al., 2003. Pressurized Coring of Near-Surface Gas-Hydrate Sediments on Hydrate Ridge: the Multiple Autoclave Corer, and First Results from Pressure-Core X-Ray CT Scans. Egs Agu Eug Joint Assembly.
- Iscan, A.G., 2021. Water saturation calculation using fractional flow and production logging data in a Caspian region sandstone petroleum reservoir. J. Petrol. Sci. Eng. 200 (5), 108355. https://doi.org/10.1016/j.petrol.2021.108355.
- Li, J.N., Xie, H.P., Chen, L., et al., 2020. Exploring deep-rock mechanics through mechanical analysis of hard-rock in situ coring system. Adv. Civ. Eng. 2020 (4), 1–11. https://doi.org/10.1155/2020/8899156.
- Li, J.Z., Tao, X.W., Bai, B., et al., 2021. Geological conditions, reservoir evolution and favorable exploration directions of marine ultra-deep oil and gas in China. Petrol. Explor. Dev. 48 (1), 60–79.
- Liu, H., Wang, S.L., Pei, X., H, et al., 2021. Development of in-situ fidelity continuous coring tools for old wells in oilfields. Acta Pet. Sin. 42 (3), 358–366 (in Chinese).
- Ma, Y.X., Li, W.H., 2016. A new saturation correction model for the samples from sealed coring wells. China Offshore Oil Gas 28 (2), 78–82 (in Chinese).
- Mcmahon, S., Ivarsson, M., 2019. A new frontier for palaeobiology: earth's vast deep biosphere. Bioessays 41 (8). https://doi.org/10.1002/bies.201900052.
- Milkov, A.V., Dickens, G.R., Claypool, G.E., et al., 2004. Co-existence of gas hydrate, free gas, and brine within the regional gas hydrate stability zone at Hydrate Ridge (Oregon margin): evidence from prolonged degassing of a pressurized core. Earth Planet Sci. Lett. 222 (3–4), 829–843. https://doi.org/10.1016/j.epsl.2004.03.028.
- Pang, X.Q., Jia, C.Z., Wang, W.Y., 2015. Petroleum geology features and research developments of hydrocarbon accumulation in deep petroliferous basins. Petrol. Sci. 12 (1), 1–53. https://doi.org/10.1007/s12182-015-0014-0.
- Schultheiss, P., Holland, M., Humphrey, G., 2009. Wireline coring and analysis under pressure: recent use and future developments of the HYACINTH system. Sci. Drill. 7, 151–163. https://doi.org/10.5194/sd-7-44-2009.
- Shale, L., Radford, S., Uhlenberg, T., et al. (Eds.), 2014. New Sponge Liner Coring System Records Step-Change Improvement in Core Acquisition and Accurate Fluid Recovery. Society of Petroleum Engineers.
- Sun, L., Zou, C., Zhu, R., et al., 2013. Formation, distribution and potential of deep hydrocarbon resources in China. Petrol. Explor. Dev. 40 (6), 687–695. https:// doi.org/10.1016/S1876-3804(13)60093-2.
- Sun, L.D., Fang, C.L., Sa, L.M., et al., 2015. Innovation and prospect of geophysical technology in the exploration of deep oil and gas. Shiyou Kantan Yu Kaifa/Petroleum Exploration and Development 42 (4), 454–465. https://doi.org/ 10.1016/S1876-3804(15)30038-0.
- Sun, S.Q., Zhang, Q., Zheng, K.G., et al., 2020. Technology and equipment of sealed coring for accurate determination of coalbed gas content in ground well. J. China Coal Soc. 45 (7), 2523–2530 (in Chinese).
- Teske, A.P., 2005. The deep subsurface biosphere is alive and well. Trends Microbiol. 13 (9), 402–404. https://doi.org/10.1016/j.tim.2005.07.004.
- Tian, J., Chen, J.Q., Jiao, J., et al., 2010. Comparison of the surface and underground natural gas occurrences in the Tazhong uplift of the Tarim Basin. Acta Geol. Sin. 84 (5), 1097–1115. https://doi.org/10.1111/j.1755-6724.2010.00283.x.
- Tu, B., Li, J., 2017. A new dynamic model for sealed coring saturation correction in hydrocarbon reservoir. Geofluids 1–8. https://doi.org/10.1155/2017/5395308, 2017.
- Wan, H., Zhao, W., Hua, X., et al., 2019. Numerical study of influence of deep coring parameters on temperature of in-situ core. Therm. Sci. 23, 209. https://doi.org/10.2298/TSCI180813209W.
- Xie, H.P., 2019. Research review of the state key research development program of China. J. China Coal Soc. 44 (5), 1283—1305 (in Chinese)
- Xie, H.P., Gao, F., Ju, Y., 2015. Research and development of rock mechanics in deep ground engineering. Chin. J. Rock Mech. Eng. 34 (11), 2161–2178 (in Chinese).
- Xie, H.P., Gao, M.Z., Zhang, R., et al., 2020. Study on concept and progress of in situ fidelity coring of deep rocks. Chin. J. Rock Mech. Eng. 39 (5), 865–876 (in Chinese).
- Xie, H.P., Liu, T., Gao, M.Z., et al., 2021. Research on in-situ condition preserved coring and testing systems. Petrol. Sci. 18 (6), 1840–1859. https://doi.org/ 10.1016/j.petsci.2021.11.003.
- Yao, J., Sun, H., Fan, D.Y., et al., 2013. Numerical simulation of gas transport mechanisms in tight shale gas reservoirs. Petrol. Sci. 10 (4), 528–537.
- Yu, B., Xie, H.P., Chen, L., et al., 2020. Exploration of digital twin design mechanism

- of the deep in situ rock insulation coring device. Geofluids 2020 (1), 1–12. https://doi.org/10.1155/2020/8835085.
- Zhao, X.Z., Jin, Q., Jin, F.M., et al., 2013. Origin and accumulation of high-maturity oil and gas in deep parts of the Baxian Depression, Bohai Bay Basin, China. Petrol. Sci. 10.(3), 303–313. https://doi.org/10.1007/s12182-013-0279-0
- Sci. 10 (3), 303—313. https://doi.org/10.1007/s12182-013-0279-0.

 Zhao, Y.Y., 2021. Investigation on washing condition of reservoir in Region A. J. Phys. Conf. 1894 (1), 012018. https://doi.org/10.1088/1742-6596/1894/1/012018.
- Zhao, Z.Y., Xie, H.P., Liu, T., et al., 2020. In situ curing of a polymer film for light-proof coring of deep rocks with preservation of rock quality and moisture. Adv. Civ. Eng. 8843779. https://doi.org/10.1155/2020/8843779, 2020.
 Zhu, H.Y., Liu, Q.Y., Deng, J.G., et al., 2013. A pressure and temperature preservation
- Zhu, H.Y., Liu, Q.Y., Deng, J.G., et al., 2013. A pressure and temperature preservation system for gas-hydrate-bearing sediments sampler. Liq. Fuel. Technol. 31 (6), 652–662. https://doi.org/10.1080/10916466.2010.531352.